Inorganic Chemistry

Article

pubs.acs.org/IC

Nonlinear-Optical Properties of α-Diiminedithiolatonickel(II) Complexes Enhanced by Electron-Withdrawing Carboxyl Groups

Luca Pilia,*[,†,‡] Maddalena Pizzotti,[§] Francesca Tessore,[§] and Neil Robertson*[,†]

[†]School of Chemistry and EaStChem, University of Edinburgh, King's Buildings, West Mains Road, Edinburgh EH9 3JJ, U.K.

[‡]Dipartimento di Ingegneria Meccanica Chimica e dei Materiali, Università di Cagliari, via Marengo 2, I09123, Cagliari, Italy

[§]Dipartimento di Chimica Inorganica Metallorganica e Analitica "Lamberto Malatesta", Università di Milano, Unità di Ricerca dell'INSTM, via G. Venezian 21, 20133 Milano, Italy

Supporting Information

ABSTRACT: We report the synthesis, characterization, nonlinear-optical (NLO) properties, and density functional theory (DFT) calculations for three nickel diiminedithiolate complexes [Ni(4,4′-R_2carboxy-bpy)(L)] [R = methyl, L = 1,2-benzenedithiolate (bdt), **1**; R = ethyl, L = 5,6-dihydro-1,4-dithine-2,3-dithiolate (dddt), **2**; R = ethyl, L = 1-(*N*-methylindol-5-yl)ethene-1,2-dithiolate (mi-5edt), **3**]. The crystal structure of **1** shows a square-planar coordination for the nickel ion and bond distances consistent with a diiminedithiolate description for the complex. For all complexes, the cyclic voltammetry measurements show two reversible reduction processes (−1.353/−1.380 V and −0798/−0.830 V, respectively) and an anodic wave (+0.372/+0.601 V). The UV−vis spectra present a band around 600−700 nm (ε = 4880−6000 dm^3 mol^{-1} cm^{-1}) mainly attributed to a charge-transfer highest occupied molecular orbital (HOMO)−lowest unoccupied molecular orbital (LUMO) transition, which shows a large negative solvatochromic shift, characteristic of push−pull complexes, and is responsible for the NLO properties of these molecules. The charge-transfer character of this electronic transition is confirmed by DFT calculations, with the HOMO mainly centered on the dithiolate moiety and the LUMO on the bpy ligand, with important contribution given by the carboxyl groups (≈13%). Small contributions from the nickel(II) ion are present in both of the frontier orbitals. The carboxyl groups enhance the optical properties of this class of complexes, confirmed by comparison with the corresponding unsubstituted compounds. The second-order NLO properties have been measured by an electric-field-induced second-harmonic-generation technique using a 10^{-3} M solution in *N*,*N*-dimethylformamide and working with a 1.907 μm incident wavelength, giving for $\mu\beta_{1.907}$ ($\mu\beta_0$) values of −1095 (−581), −2760 (−954), and −1650 (−618) × 10^{-48} esu for **1**−**3**, respectively. These values are among the highest in the class of square-planar push−pull complexes, similar to those found for dithionedithiolate compounds. Moreover, spectroelectrochemical experiments demonstrate the possibility of using these complexes as redox-switchable NLO chromophores.

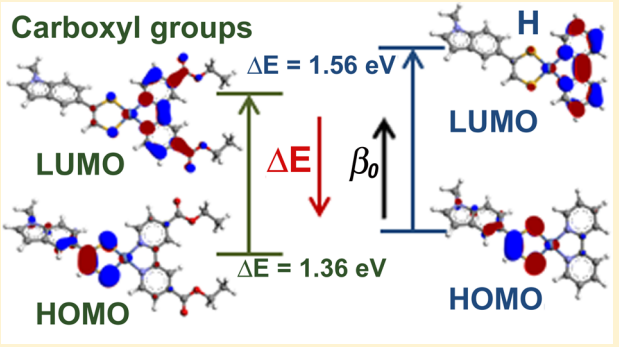

INTRODUCTION

Molecular materials showing second-order (β) nonlinear-optical (NLO) properties have received much interest for their possible application in optoelectronic and photonic devices,[1] because of their large NLO response, fast response time, and, moreover, easy processability for device fabrication. Many molecular NLO chromophores have been proposed so far, both organic[1b,2] and inorganic; in the latter case, push−pull and octupolar type complexes of several transition's metals with high β values have been reported.[3] The possibility of switching the NLO properties plays a very important role in order to make these materials suitable for many applications. Since the first reversible redox switching of the NLO property was demonstrated by Coe et al.,[4] other kinds of switching, such as protonation,[5] light-induced isomerization,[6] and ion capture,[7] have been reported besides the redox ones.[8] Furthermore, in order to achieve an electric or a magnetic switch of the NLO properties, various multifunctional materials, which in addition to NLO show conducting[9] or magnetic properties,[10] have been reported.

The second-order NLO properties of asymmetric push−pull metal d^8 complexes have been extensively studied in the last decades, and several of them show high values of the first molecular hyperpolarizability (β). The class of square-planar metal(II) diiminedithiolate compounds (metal M = Ni, Pd, and Pt) presents various properties: redox activity,[11] NLO,[12] and photoluminescence in solid and solution states.[12a13] Furthermore, the platinum complexes show long-lifetime excited states[13,14] and electron transfer,[13a] which make these compounds suitable for solar cells[15] and photocatalytic applications.[14] Indeed, the photogeneration of dihydrogen by

Received: January 27, 2014
Published: April 24, 2014

   dx.doi.org/10.1021/ic5002094 | *Inorg. Chem.* 2014, 53, 4517−4526

water splitting using an integrated system based on TiO_2 and their platinum derivatives as sensitizers has recently been achieved.[16]

Eisenberg and co-workers have studied the structure−property relationship in the second harmonic generation in metal diiminedithiolato complexes.[12] The NLO properties arise from the charge-transfer (CT) character of the highest occupied molecular orbital (HOMO)−lowest unoccupied molecular orbital (LUMO) transition, which falls in the visible region of the spectrum with a medium molar absorption coefficient and a large solvatochromism. The origin of the CT character and consequently of the solvatochromism was attributed, both theoretically and experimentally, to the different electronic structures of the frontier orbitals. In fact, the LUMO is mostly based on the diimine ligand, while the HOMO is composed mainly of the dithiolate moiety (some contributions from the metal orbitals are also observed); consequently, a ligand-to-ligand charge-transfer (LLCT) or mixed-metal ligand-to-ligand charge-transfer (MMLLCT) character can be assigned to this transition. A schematic description of the ground (A) and excited (B) states is reported in Scheme 1; the dithiolate ligand, which is easy to oxidize, acts

Scheme 1. Schematic Representation of the Ground (A) and Excited (B) States of a Nickel Diiminedithiolate Complex

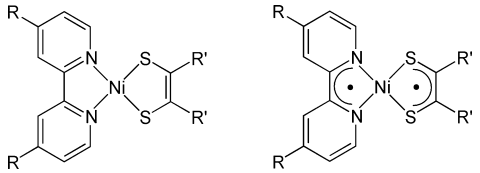

as a donor, while the diimine moiety acts as an acceptor, being easier to reduce.[12b,17] The transition energy and molecular dipole can be tuned by modifying the peripheral substituents. The presence of electron-withdrawing (electron-donating) groups lowers (increases) the energies of the orbitals, and the *push−pull* (acceptor−donor) capability of the two ligands can be tuned by an appropriate choice of the substituents. The optical absorption can be also tuned by changing the metal ion. A similar description of the electronic structures has been used with the dithionedithiolate compounds, another class of *push−pull* mixed-ligand complexes that show NLO properties;[18] in this case, a 1,4-dialkylpiperazine-2,3-dithione molecule is used instead of a diimine molecule as the acceptor ligand. Recently, Deplano et al. have investigated the metal,[19] dithiolate,[19,20] and dithione[21] effects on the NLO properties of this class, and they found values of β similar to those of the diiminedithiolato complexes reported so far.[22]

Although a simplification, the two-state model[23] (eq 1) provides a relationship between the features of the molecules (such as dipole moments and optical transition) and β, for both of these classes of chromophores,[12b,14b,18,19] as well as for organic CT compounds.[2a] Equation 1 shows the relationship between β_0 (the static quadratic hyperpolarizability), λ_{max} (the maximum of the HOMO−LUMO transition), f (the oscillator strength), and the difference between the ground- and excited-state dipole moments ($\Delta\mu$).

$$\beta_0 = 1.617\lambda_{max}{}^3 f \Delta\mu \quad (1)$$

The value of β_0 is heavily influenced by the electronic transition energy (by a cubic dependence); therefore, the presence on the molecule of groups able to reduce the HOMO−LUMO gap is expected to increase the β_0 value.

In this study, we report the preparation, characterization, and NLO properties of three nickel(II) diiminedithiolate complexes; the diimine ligand is 2,2′-bipyridine (bpy; see Chart 1)

Chart 1

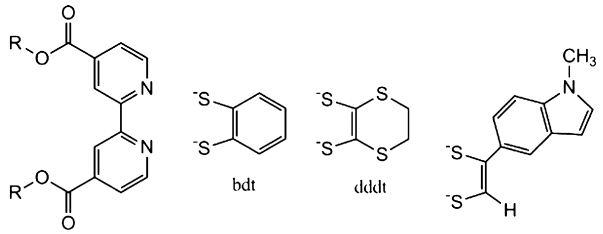

bearing two dialkylcarboxy groups, in the 4 and 4′ positions, in order to lower the energy of the ligand's orbitals (especially those of the LUMO) and in this way to increase λ_{max} and, consequently, β. As dithiolate ligands (Chart 1), benzene-1,2-dithiolate (bdt), 5,6-dihydro-1,4-dithine-2,3-dithiolate (dddt), and 4-(1-methyl-5-indol-5-yl)[1,3]dithiolate (mi-5edt) were used. Although the first of these has been previously used as a donor ligand in these types of compounds,[12] the bpy moiety was always unsubstituted or contained donor groups, except for some platinum chromophores.[13b,16]

The presence of the carboxyl groups on the complexes gives the possibility of anchoring these molecules onto inorganic oxide supports or electrodes[16] in order to prepare NLO and electrooptical devices. Moreover, attaching the complexes onto a surface will align them, avoiding a centrosymmetric, solid-state organization, which would suppress the NLO properties at the molecular level.

Furthermore, we report the first example of a mixed-ligand complex of mi-5edt, for which the symmetric neutral compound has been shown to form thin films by electropolymerization.[24]

EXPERIMENTAL SECTION

Materials and Reagents. All reagents were purchased from Sigma-Aldrich and used as received without further purification. 4,4′-Diethylcarboxy-2,2′-bipyridine,[25] 2,5,7,9-tetrathiabicyclo[4.3.0]non-1(6)-en-8-one (TTBEO),[26] and 4-(1-methyl-5-indol-5-yl)[1,3]-dithiol-2-one were prepared as previously reported. [Ni(4,4′-diethylcarboxy-bpy)Cl_2]·H_2O was synthesized following Brewer's method using methanol (MeOH) instead of ethanol (EtOH).[27] The reactions were carried out under a nitrogen atmosphere and using anhydrous solvents.

[Ni(4,4′-dimethylcarboxy-bpy)(bdt)] (1). A total of 69.5 mg (0.49 mmol) of benzene-1,2-dithiol was added to 10 mL of a 0.1 M methanol (MeOH) solution of MeONa; the resulting solution was slowly added to 219 mg (0.49 mmol) of [Ni(4,4′-dimethylcarboxy-bpy)Cl_2]·H_2O dissolved in 20 mL of MeOH. Immediately a green precipitate appeared. After 2 h of stirring, the solid was collected by filtration and washed three times with MeOH (170 mg). Yield: 74%. Analytical results are in accordance with the formula [Ni(4,4′-dimethylcarboxy-bpy)(bdt)]. Anal. Calcd for $C_{20}H_{16}N_2NiO_4S_2$: C, 50.98; H, 3.42; N, 5.95. Found: C, 50.62; H, 3.37; N, 5.84. UV−vis [in DMF; λ, nm (ε, dm^3 mol^{-1} cm^{-1})]: 318 (14000), 387 (3830), 434sh, 610 (4880). IR (cm^{-1}): 3056vw, 29949w, 2918w, 2851w, 2591vw,

dx.doi.org/10.1021/ic5002094 | Inorg. Chem. 2014, 53, 4517−4526

1728s, 1618mw, 1557mw, 1432ms, 1402m, 1361w, 1323ms, 1294ms, 1250s, 1237s, 1192w, 1124ms, 1065w, 1050w, 1018mw, 976mw, 960m, 909vw, 898vw, 876w, 860w, 842w, 785w, 758s, 739m, 722m, 699s, 677mw, 67mw, 596mw, 569vw, 555vw, 549vw, 532mw, 525m, 516vs, 510vs.

[Ni(4,4′-diethylcarboxy-bpy)(dddt)] (**2**). A total of 80 mg (0.38 mmol) of TTBEO was added to 15 mL of a 0.05 M EtOH solution of EtONa; the resulting solution was added to 172 mg (0.38 mmol) of [Ni(4,4′-diethylcarboxy-bpy)Cl_2]·H_2O dissolved in 60 mL of warm acetonitrile. Immediately a dark green precipitate appeared. After 2 h of stirring, the solid was collected by centifugation and washed with EtOH (two times), MeOH (three times), and Et_2O (three times) (128 mg). Yield: 62%. Analytical results are in accordance with the formula [Ni(4,4′-diethylcarboxy-bpy)(bdt)]. Anal. Calcd for $C_{20}H_{20}N_2NiO_4S_4$: C, 44.54; H, 3.74; N, 5.09. Found: C, 44.42; H, 3.68; N, 5.09. UV−vis [in DMF; λ, nm (ε, dm^3 mol^{-1} cm^{-1})]: 330 (21600), 390sh, 445 (3000), 735 (6000). IR (cm^{-1}): 3080vw, 2980w, 2927w, 2901w, 2871vw, 2820vw, 2750vw, 1721ms, 1618w, 1554w, 1515w, 1474mw, 1439w, 1407ms, 1364m, 1315m, 1299ms, 1209ms, 1234s, 1172mw, 1139m, 1124ms, 1109ms, 1063mw, 1023ms, 1015ms, 982w, 920w, 887w, 870mw, 860mw, 809vw, 773w, 756s, 703s, 685w, 666w, 652vw, 556mw, 533w, 526w, 517s, 507s, 512vs, 505vs.

[Ni(4,4′-diethylcarboxy-bpy)(mi-5edt)] (**3**). **3** was prepared as reported above for the corresponding dddt complex using the following amounts: 100 mg (0.40 mmol) of 4-(1-methyl-5-indol-5-yl)[1,3]dithiol-2-one in 16 mL of a 0.05 M EtOH solution of EtONa and 179 mg (0.40 mmol) of [Ni(4,4′-diethylcarboxy-bpy)Cl_2]·H_2O in 60 mL of warm CH_3CN, obtaining 130 mg of product. Yield: 62%. Analytical results are in accordance with the formula [Ni(4,4′-diethylcarboxy-bpy)(mi-5edt)]. Anal. Calcd for $C_{27}H_{25}N_3NiO_4S_2$; C, 56.07; H, 4.36; N, 7.27. Found: C, 55.68; H, 4.24; N, 7.17. UV−vis [in DMF; λ, nm (ε, dm^3 mol^{-1} cm^{-1})]: 325 (22200), 380sh, 445 (4180), 716 (5100). IR (cm^{-1}): 2867w, 2816vw, 1721vs, 1614w, 1554m, 1506mw, 1472m, 1434mw, 1405ms, 1365m, 1316s, 1303ms, 1256vs, 1237vs, 1143ms, 1129ms, 1115ms, 1067mw, 1021s, 957w, 933w, 889m, 878m, 861m, 849mw, 816vw, 797m, 776ms, 758vs, 728ms, 714vs, 702s, 665mw, 653m, 632w, 593m, 567mw, 532w, 519 ms, 509vs.

IR spectra (4000−500 cm^{-1}) were recorded on a PerkinElmer Spectrum 65 FT-IR spectrometer. Electronic spectra were recorded with a PerkinElmer Lambda 9 spectrophotometer, controlled by a datalink PC, running *UV/Winlab* software recorded in a solution of DMF, using a quartz cell of path length 1 cm. Elemental analysis were performed with a Carlo Erba CE1108 elemental analyzer. Cyclic voltammograms were carried out on an μAUTOLAB Type III potentiostat, driven by *GPES* electrochemical software, using a conventional three-electrode cell consisting of platinum wire as the working electrode, platinum wire as the counter electrode, and Ag/AgCl in a saturated LiCl/EtOH solution as the reference electrode. The experiments were performed at room temperature (25 °C), in dry and argon-degassed DMF containing 0.1 mol dm^{-3} Bu_4NPF_6 as the supporting electrolyte, at a 25−200 mV s^{-1} scan rate. The half-wave potential for a ferrocene/ferrocenium (Fc/Fc^+) couple (internal standard) is +0.544 V under the above conditions. Spectroelectrochemistry measurements were performed at room temperature by an optically transparent thin layer electrochemistry (OTTLE) technique in dry and argon-degassed DMF containing 0.1 mol dm^{-3} Bu_4NPF_6 as the supporting electrolyte using a 0.5 mm quartz cell at −1.0 and +0.1 V for the reduction and oxidation processes, respectively. The UV−vis−near-IR (NIR) spectra were recorded with a Jasco V-670 spectrophotometer.

Electric-field-induced second-harmonic-generation (EFISH) experiments[28] were performed using for each complex a freshly prepared 10^{-3} M solution in DMF and working with a 1.907 μm incident wavelength, obtained by Raman shifting the 1.064 μm emission of a Q-switched Nd:YAG laser in a high-pressure hydrogen cell (60 bar). A liquid cell with thick windows in the wedge configuration was used to obtain the Maker fringe pattern (harmonic intensity variation as a function of liquid cell translation). In the EFISH experiments, the incident beam was synchronized with a direct-current field applied to the solution, with 60 and 20 ns pulse duration, respectively, in order to break its centrosymmetry. From the concentration dependence of the harmonic signal with respect to that of the pure solvent, the NLO responses were determined (assumed to be real because the imaginary part was neglected) from the experimental value γ_{EFISH}, through eq 2:

$$\gamma_{EFISH} = \frac{\mu\beta_\lambda(-2\omega;\,\omega,\,\omega)}{5kT} + \gamma(-2\omega;\,\omega,\,\omega,\,0) \qquad (2)$$

where γ_{EFISH} is the sum of a cubic electronic contribution $\gamma(-2\omega;\omega,\omega,0)$ and of a quadratic orientational contribution $\mu\beta_\lambda(-2\omega;\omega,\omega)/5kT$, with μ being the ground-state dipole moment and β_λ the projection along the dipole moment direction of the vectorial component β_{vec} of the tensorial quadratic hyperpolarizability working with the incident wavelength λ.

A summary of data collection and structure refinement for **1** is reported in Table 1. Single-crystal data were collected with a SuperNova, dual, copper at zero, Atlas, Mo Kα: λ = 0.71073 Å. The unit cell parameters were obtained using 60 ω frames of 0.5° width and scanned from three different zones of the reciprocal lattice. The intensity data were integrated from several series of exposure frames (0.3° width) covering the sphere of reciprocal space.[29] A semiempirical from equivalents absorption correction was applied using the program *SADABS*[30] with min and max transmission factors of 0.61−0.97. The structures were solved by direct methods (*SIR92*)[31] and refined on F^2 with full-matrix least squares (*CRYSTALS*).[32] Non-hydrogen atoms were refined anisotropically, and the hydrogen atoms were placed at their calculated positions. Graphical material was prepared with the *Mercury 2.0* program.[33] CCDC 975351 contains the supplementary crystallographic data for this paper.

Table 1. Summary of X-ray Crystallographic Data for 1

empirical formula	$C_{20}H_{16}N_2NiO_4S_2$
fw	471.20
color, habit	black, block
cryst size, mm	0.131 × 0.060 × 0.024
cryst syst	monoclinic
space group	*C*12/*c*1
a, Å	31.416(6)
b, Å	7.5820(7)
c, Å	20.608(4)
β, deg	128.27(3)
V, Å^3	3853.9(2)
Z	8
T, K	100
ρ(calcd), Mg m^{-3}	1.624
μ, mm^{-1}	1.254
θ range, deg.	2.518 to 28.586
no.of reflns/unique reflns	19821/4333
GOF	0.9543
R1	0.0380
wR2	0.0735

R1 = $\sum||F_o| - |F_c||/\sum|F_o|$; wR2 = $[\sum[w(F_o^2 - F_c^2)^2]/\sum[w(F_o^2)^2]]^{1/2}$, where $w = 1/[\sigma^2(F_o^2) + (aP)^2 + bP]$ and $P = [\max(F_o^2,0) + 2F_c^2]/3$.

Ground-state electronic structure calculations of complexes **1**−**3** were performed at the density functional theory (DFT)[34] level employing the *Gaussian 09*[35] software package. The functionals used throughout this study were B3LYP,[36,37] CAM-B3LYP,[38] and PBE1PBE.[39] The ground-state geometries were obtained in the gas phase by full geometry optimization without any symmetry constraint; in the case of complex **1**, geometry optimization was also performed starting from the structural data. The basis set employed for all atoms was the valence triple-ζ 6-311+G(d,p).[40] All structures were input through the *ArgusLab 4.0* program.[41] The atomic orbital composition was calculated using Mulliken population analysis.

dx.doi.org/10.1021/ic5002094 | *Inorg. Chem.* 2014, 53, 4517−4526

To take into account the compounds' interaction with the solvent's electric field, the polarizable conductor continuum model (CPCM), as implemented in *G09*,[39] was used. The 10 lowest singlet excited states of the closed-shell complexes were calculated within the time-dependent DFT (TDDFT) formalism, as implemented in *Gaussian*,[42] in a DMF-simulated electric field (parameters: ε = 37.21, molar volume = 77.41, density = 0.0079, solvent radius = 2.647 Å). Calculations in acetone-, dichloromethane-, acetonitrile-, and chloroform-simulated electric fields were also performed. In order to evaluate $\mu\beta_0$ with the two-state model (eq 1), the differences between the dipole moments of the excited state and that of the ground state ($\Delta\mu_{ge}$) were calculated by a simulated Stark effect, taking into account the difference in the lowest transition's energies, calculated with and without an external electric field of ±0.0005 au of strength.[43] These calculations were done by TDDFT methods in the gas phase and DMF as well.

The optimized molecular structures and orbital isosurfaces were visualized using *ArgusLab 4.0*.[41]

RESULTS AND DISCUSSION

Synthesis. Complex **1** was prepared by adding a sodium salt of benzene-1,2-dithiol in MeOH to a solution of [Ni(4,4′-diethylcarboxy-bpy)Cl_2]·H_2O in the same solvent. Surprisingly, instead of the expected diethylcarboxy-substituted compound, the corresponding dimethyl one was obtained, probably because of the small excess of base MeO^- used to prepared the dithiolate salt that catalyzed the trans-esterification reaction. In order to avoid this problem, complexes **2** and **3** were synthesized starting from an EtOH solution of the sodium salt of the dithiolene ligand, added to a warm solution of [Ni(4,4′-diethylcarboxy-bpy)Cl_2]·H_2O in acetonitrile (see Scheme 2).

Scheme 2

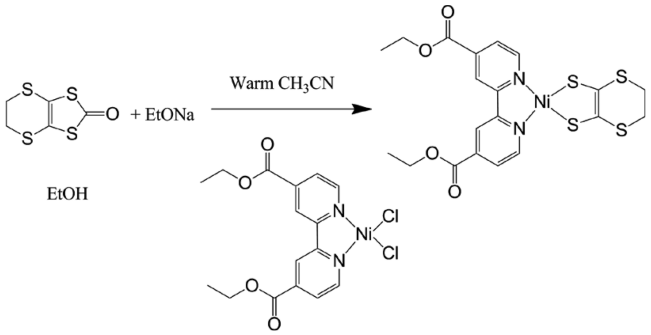

X-ray Characterization. Single crystals of **1** suitable for X-ray characterization were obtained by slow evaporation of a CH_2Cl_2 solution. A summary of crystallographic data for **1** are reported in Table 1. Figure 1 shows a representation of the molecule. The nickel ion is in square-planar coordination, with the largest deviation from the calculated plane between the atoms of the core (S2−S9−Ni1−N10−N21) observed for N21 (0.039 Å). Also, the ligands are almost coplanar, and the angle between the calculated planes defined by S2−C3−C8−S9 and N10−C11−C20−N21 for the bdt and bpy ligands, respectively, is 3.11°.

The bond distances reported in Table 2 are similar to those previously found in a similar complex.[44] The molecules are arranged in dimers, with a head−tail orientation, as expected because of the dipole moment. Only two intradimer S2···C26′ and C26···S2′ short contacts of 3.460 Å are present (Figure 2), while several interdimer H···O, C···O, and H···C distances shorter than the sum of the van der Waals radius are present.

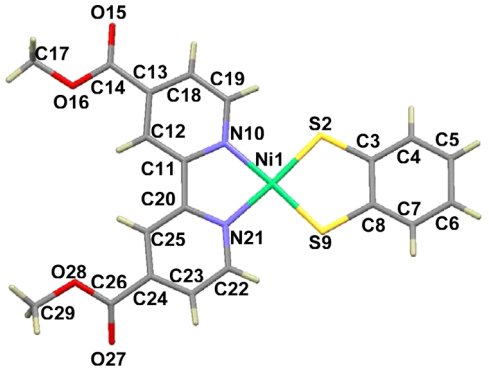

Figure 1. **1** with atomic numbering.

Table 2. Selected Bond Lengths (Å) and Angles (deg) for 1

Ni1−S2	2.1509(8)	N21−C22	1.354(3)
Ni1−S9	2.143(1)	C11−C20	1.461(3)
Ni1−N10	1.930(2)	S2−Ni1−S9	90.37(5)
Ni1−N21	1.937(2)	S2−Ni1−N10	92.65(7)
C3−S2	1.740(3)	N10−Ni1−N21	83.55(9)
C8−S9	1.755(3)	S9−Ni1−N21	93.44(7)
C3−C8	1.391(3)	Ni1−S2−C3	106.44(9)
N10−C11	1.359(3)	S2−C3−C8	118.5(2)
N10−C19	1.346(3)	Ni1−N10−C11	114.2(2)
N21−C20	1.360(3)	N10−C11−C20	114.1(2)

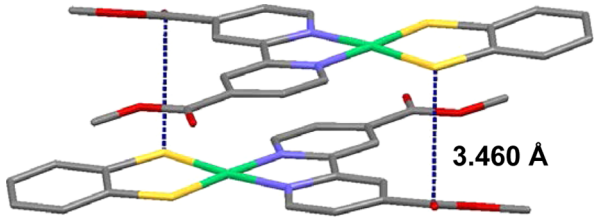

Figure 2. Dimer with head-to-tail arrangement of **1**.

Along the *b* axis, there are layers of alternating dimers perpendicular to the *ab* plane (Figures S1 and S2 in the Supporting Information, SI).

UV−Vis−NIR Spectroscopy. The electronic spectra show a medium-intensity broad band in the vis−NIR region with an absorption maximum (ε, $dm^3\ mol^{-1}\ cm^{-1}$) at 610 (4880), 735 (6000), and 716 (5100) nm for **1**−**3**, respectively (Figure 3).

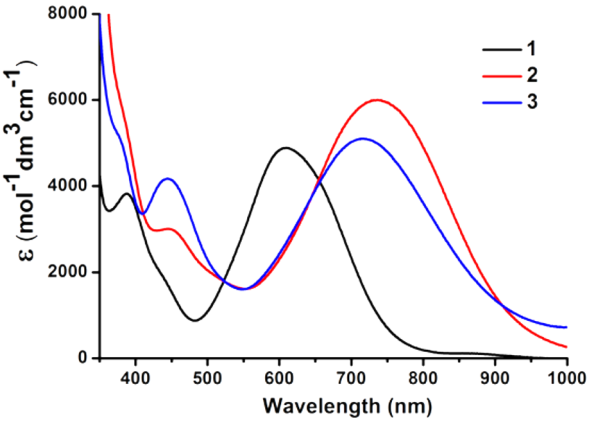

Figure 3. UV−vis−NIR spectra in a DMF solution of **1**−**3**.

dx.doi.org/10.1021/ic5002094 | *Inorg. Chem.* 2014, 53, 4517−4526

This absorption has been assigned to a HOMO−LUMO transition and presents a large negative solvatochromic effect, as shown in Figures 4 and S3 and S4 in the SI for **1**−**3**,

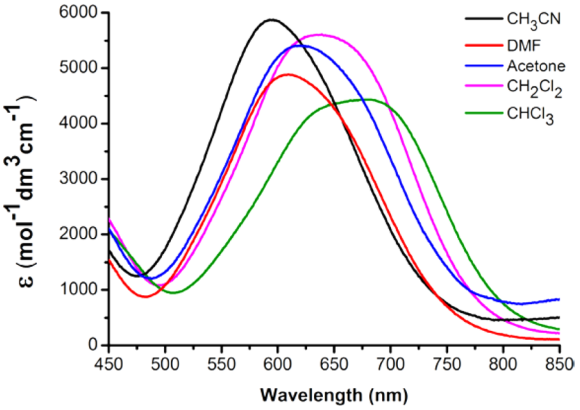

Figure 4. Solvatochromic effect of complex **1** in CH_3CN, DMF, acetone, CH_2Cl_2, and $CHCl_3$.

respectively, which confirms the CT character associated with this transition (the negative sign of the solvatochromism is due to the smaller dipole moment in the excited state compared to that of the ground state). In chloroform, for **1**, this band falls at 670 nm and in the analogous complex with an unsubstituted bpy ligand (**1′**) at 557 nm[14b,44] (difference ≈ 3030 cm^{-1}). As expected, the electron-withdrawing carboxyl groups on the bpy ligand lower the energy of the LUMO, reducing the HOMO−LUMO gap. Moreover, the absorption intensity in the case of **1** (ε = 4400 dm^3 mol^{-1} cm^{-1} in $CHCl_3$) is higher than that of **1′** (ε = 2500 dm^3 mol^{-1} cm^{-1}).[14b] Both of these findings, the transition energies and intensity (the intensity is related to the oscillator strength, *f*), make the carboxyl-substituted compound more promising as an NLO chromophore than the unsubstituted one (see eq 1). For all of the complexes, the energies of the maxima of the solvatochromic bands show a linear behavior versus solvent polarity parameters (r^2 > 0.967), as proposed by Cummings and Eisenberg for several platinum diiminedithiolate complexes[13b] (Figure S5 in the SI); the solvatochromic shifts, obtained from the plot's slope, are similar to those found for the platinum compounds[13b] ranging from 0.478 to 0.586.

Electrochemical Characterization. The cyclic voltammetry measurements performed in DMF solutions show for all three complexes two reversible reduction waves at around −0.80 and −1.36 V for the 0 ⇆ 1− and 1− ⇆ 2− processes, respectively (Table 3 and Figure 5, where the cyclic

Table 3. Cyclic voltammetric Data[a]

complex	$E_{1/2}$ (V)[b] for 1− ⇆ 2−	$E_{1/2}$ (V)[b] for 0 ⇆ 1−	E (V)[c] for 0 → 1+
[Ni(4,4′-dimethylcarboxy-bpy)(bdt)] (**1**)	−1.353 (79)[d]	−0.798 (69)[d]	+0.601
[Ni(4,4′-diethylcarboxy-bpy)(dddt)] (**2**)	−1.354 (80)[d]	−0.800 (70)[d]	+0.372
[Ni(4,4′-diethylcarboxy-bpy)(mi-5edt)] (**3**)	−1.380 (80)[d]	−0.830 (72)[d]	+0.444

[a]Measured at a platinum electrode in DMF, 0.1 M Bu_4NPF_6, and a scan rate of 100 mV s^{-1} (reference electrode Ag/AgCl; ferrocene internal reference $E_{1/2}$ = 0.544 V, ΔE_p = 72 mV). [b]Reversible. [c]Irreversible anodic wave. [d]Peak-to-peak separation ΔE_p (mV).

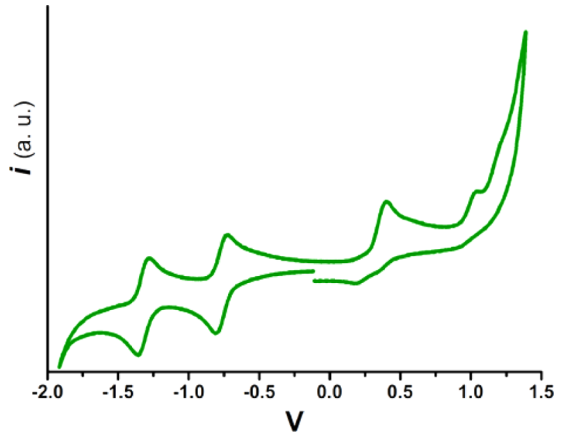

Figure 5. Cyclic voltammogram of **2** in a DMF degassed solution, containing 0.1 mol dm^{-3} Bu_4NPF_6 at a scan rate of 0.100 V s^{-1}.

voltammogram of **2** is shown as an example). Moreover, an irreversible anodic peak is present at +0.601 V (**1**), +0.372 V (**2**), and +0.444 V (**3**). While the reduction processes fall at similar potentials, the oxidation waves appear at different positions, in agreement with a description of the frontier orbitals, which considers the LUMO (involved in the reduction processes) mainly due to the bpy moiety and the HOMO (involved in the oxidation) mostly composed by the dithiolene ligand orbitals. This is in agreement with the computational results (vide infra).

The [Ni(bpy)(bdt)] complex[44,45] shows (in benzonitrile) the first reduction process at −1.333 V and the anodic wave at +0.580 V. Compared with those found for **1**, the latter electrochemical potential is very similar, while the reduction is more difficult for the unsubstituted compound, confirming the strong electron-withdrawing effect due to the carboxyl groups.

The reversibility of the first reduction process and the high stability of the monoanion produced allowed us to perform spectroelectrochemical measurements at room temperature. As expected, the formation of the monoreduced species (Figures 6 and S7-A in the SI) changes the electronic spectra. In fact, a new band appears in the NIR region, while the corresponding depletion of the neutral complex is shown by bleaching of the solvatochromic peak, which corresponds to the electronic transition mainly responsible for the NLO properties. The application of a small positive potential (+0.1 V) induces the

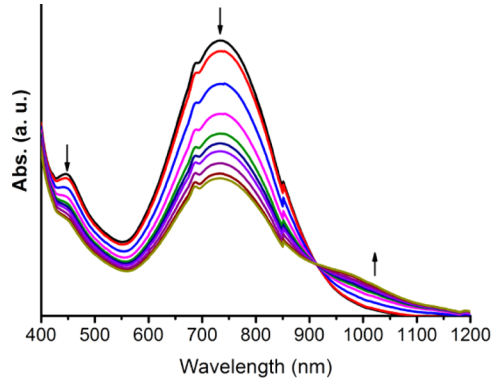

Figure 6. OTTLE of complex **3** under reductive conditions, showing the formation of a stable anion with vis−NIR absorption at lower energy than **3** (the jumps at 680 and 850 nm are artifacts of the spectrophotometer).

dx.doi.org/10.1021/ic5002094 | Inorg. Chem. 2014, 53, 4517−4526

reoxidative process with restoration of the band characteristic of the neutral species (Figures S6 and S7-B in the SI). The redox bistability presented by these chromophores can be interesting to make redox-switchable molecular NLO devices.[4,8]

NLO PROPERTIES

The NLO responses of the three compounds have been measured by EFISH experiments[28] in a DMF solution and working with a 1.907 μm incident wavelength. By EFISH, it is possible to measure the scalar product $\mu\beta_\lambda$, where μ represents the molecular dipole moment and β_λ the vector part of the quadratic hyperpolarizability tensor dependent on the frequency of the incident light. The experimental values for $\mu\beta_\lambda$ are reported in Table 4 together with the HOMO−LUMO

Table 4. Summary of the HOMO−LUMO Absorption Bands and Quadratic NLO Activity[a] of Complexes 1−3

complex	HOMO−LUMO λ_{max} (nm) [ε (dm^3 mol^{-1} cm^{-1})]	$\mu\beta_{1.907}$[b]	$\mu\beta_0$[b]
[Ni(4,4′-dimethylcarboxy-bpy)(bdt)]	610 [4880]	−1095	−581
[Ni(4,4′-diethylcarboxy-bpy)(dddt)]	735 [6000]	−2760	−954
[Ni(4,4′-diethylcarboxy-bpy)(mi-5edt)]	716 [5100]	−1650	−618

[a]Measured at 1.907 μm using a DMF solution by the EFISH technique; the uncertainty of the measurement is between ±5 and ±10%. [b]$\times 10^{-48}$ esu.

absorption bands mainly responsible of the NLO response. The calculated $\mu\beta_0$ values are also reported (β_0 is the static quadratic hyperpolarizability and is the extrapolated value to zero frequency). The $\mu\beta_0$ values were calculated by applying eq 3[28]

$$\mu\beta_0 = \mu\beta_\lambda[1 - (2\lambda_{max}/\lambda)^2][1 - (\lambda_{max}/\lambda)^2] \quad (3)$$

where λ is the wavelength of the incident light (1907 nm) and λ_{max} is the wavelength of the maximum of the absorption of the CT transition of the chromophore (see Table 4).

These complexes exhibit large negative first hyperpolarizabilities (Table 4) among the highest for square-planar complexes, similar to those found recently for the [Ni(dithione)(dithiolate)] class.[19,20] These values of $\mu\beta_0$ are also larger than those reported so far for d^8 metal diiminedithiolate complexes;[12] indeed, the maximum value of -480×10^{-48} esu was achieved in DMSO for [Pt(dpphen)(dtbdt)] (dpphen = 4,7-diphenylphenanthroline and dtbdt = di-*tert*-butylbenzene-1,2-dithiolate).[46] This is striking in the context that both theoretical[14b] and experimental[19a,b,20] studies have demonstrated that platinum chromophores show higher NLO responses compared to those of the other metals of the nickel triad.

CALCULATIONS

DFT calculations at the B3LYP/6-311+G(d,p) level of theory were performed to elucidate the electronic structures of the three complexes. The optimized geometries in the gas phase are shown in Figure S8 in the SI (perpendicular to the molecular plane) and Figures S9−S11 in the SI (along the plane). The geometries calculated for complexes **2** and **3** are planar. For **1**, calculations performed using the same methodology led to some deviation from planarity, however, starting from the crystallographic data gave a planar geometry similar to that seen for **2** and **3**. Both calculated conformations show excellent agreement in comparing the bond lengths and angles to the experimental data (Tables 2 and 5). The bond distances are

Table 5. Selected Calculated Bond Lengths (Å) and Angles (deg) for 1[a]

Ni-S	2.157; *2.171*	S-C(11)-C(11′)	118.38; *118.23*
Ni-N	1.900; *1.963*	S-Ni-N	94.25; *93.75*
C-S	1.764; *1.763*	Ni-N-C(1)	114.34; *114.27*
C(11)-C(11′)	1.405; *1.401*	N-C(1)-C(1′)	113.44; *114.45*
N-C(1)	1.366; *1.360*		
N-C(2)	1.354; *1.347*		
C(1)-C(1′)	1.460; *1.465*		
S-Ni-S	91.23; *89.93*		
N-Ni-N	84.26; *82.57*		
Ni-S-C(11)	105.99; *106.81*		

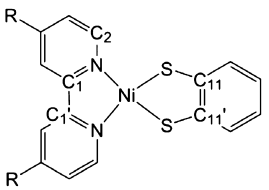

[a]The data reported in normal and italic characters refer to the calculations performed starting from the molecule modeled with the *ArgusLab 4.0.1* program and crystallographic data, respectively.

reproduced within 0.03 Å, whereas the differences between the angles are less than 0.86°, except for S−Ni−N, which is overestimated by 1.6° in the case of the distorted geometry. All further discussion of **1** below is based on the calculations started from the crystallographic data.

The frontier orbitals of **3** are shown in Figure 7, and those for **1** and **2** are reported in Figures S12 and S13 in the SI. HOMO and LUMO are both π orbitals, and in agreement with the experimental results, they are mainly formed by the orbitals of the dithiolate and bpy moieties, respectively, with small contributions from the metal (see Figure 8). In particular, the HOMO is dominated by a bonding interaction between the carbon atoms of the dithiolene core and an antibonding interaction between these carbons and the sulfur atoms. The LUMO is more delocalized, with important contributions from the nitrogen atoms antibonding with the Ni d orbital and the C=C double bond. The composition of the frontier orbitals confirms a *push−pull* description for these complexes (Table S1 in the SI). It is worth noting that the contributions of the carboxyl groups to the LUMO (14% for **1** and 13% for **2** and **3**) confirm, in agreement with the experimental findings, that the presence of these electron-withdrawing substituents significantly affects this orbital. To elucidate the effect of the carboxyl groups, DFT calculations were done with hydrogen atoms instead of the CO_2R substituents (see Table S2 in the SI). The carboxyl groups lower the energies of both of the frontier orbitals, but this effect is more pronounced for the LUMOs, reducing the gap and, consequently, increasing the λ_{max} value of the HOMO−LUMO transition. Furthermore, the oscillator strength associated with this electronic transition increases in the complexes with electron-withdrawing substituents. These findings are in agreement with the experimental results,[14b,44] and all of them favor an enhancement of the second-order NLO properties in the carboxylated compounds compared to the corresponding unsubstituted compounds (see eq 1).

To evaluate the effect of the solvent on the molecular orbitals and energy levels, DFT calculations were performed in a DMF-simulated electric field (Tables S1 and S3 in the SI). Both the energy and composition of the orbitals are affected by the

dx.doi.org/10.1021/ic5002094 | Inorg. Chem. 2014, 53, 4517−4526

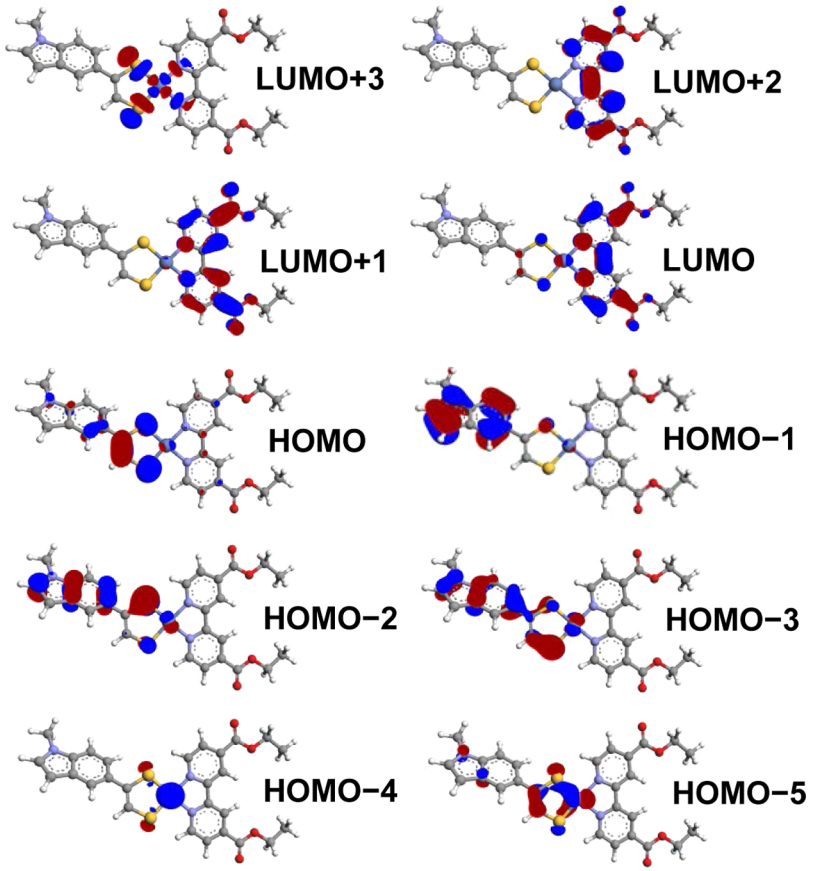

Figure 7. Frontier orbitals for **3** calculated at the B3LYP/6-311+G(d,p) level of theory and plotted with a contour value of 0.040.

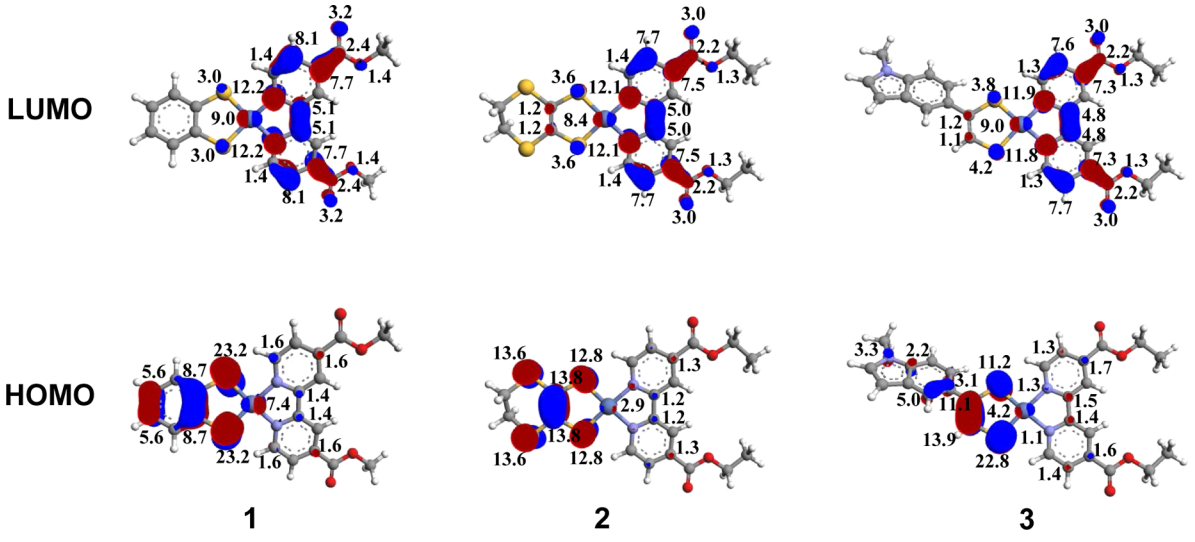

Figure 8. HOMO and LUMO orbitals' compositions expressed as percentages, calculated by the DFT calculation method at the B3LYP/6-311+G(d,p) level of theory and plotted with a contour value of 0.040.

solvent. The energy-level diagram reported in Figure S14 in the SI shows a comparison between the calculated energies in the gas phase and in DMF: solvation causes an important stabilization of the HOMO energies (≈0.5 eV), while the LUMOs are much less affected. Indeed, the LUMO orbital is destabilized in the case of **1** (by 0.154 eV), almost unchanged for **2** and slightly stabilized for **3** (0.063 eV). In agreement with the electrochemical results, the energies of the LUMOs of the three compounds are very similar (within ≈0.04 eV), whereas those of the HOMOs are much more different (0.49 eV). Solvation influences the composition of the frontier orbitals in the same way in the three complexes (Table S1 in the SI): in the HOMOs (LUMOs), the population of the dithiolate and metal orbitals increases (decreases) and, consequently, the contribution from the bpy ligand decreases (increases). The increase of the ground-state polarity due to the solvent is also confirmed by enhancement of the calculated dipolar moments in DMF compared to those in the gas phase (see Table 6).

dx.doi.org/10.1021/ic5002094 | Inorg. Chem. 2014, 53, 4517−4526

Table 6. HOMO and LUMO Energies and Dipole Moments of Complexes 1−3 Calculated by DFT[a]

complex	HOMO (eV)	LUMO (eV)	μ (D)
[Ni(4,4′-dimethylcarboxy-bpy)(bdt)]	−5.450	−3.236	17.51 (11.15)[b]
[Ni(4,4′-diethylcarboxy-bpy)(dddt)]	−4.957	−3.271	16.29 (9.25)[b]
[Ni(4,4′-diethylcarboxy-bpy)(mi-5edt)]	−5.021	−3.229	13.59 (8.07)[b]

[a]The calculations have been performed in a DMF-simulated electric field and at the B3LYP/6-311+G(d,p) level. [b]Calculated in the gas phase.

TDDFT calculations were performed to investigate the characteristics of the electronic transitions, which are summarized in Table S4 in the SI. The maxima of all of the absorptions are overestimated (more than 100 nm), especially those at the lowest energy, but qualitatively they follow the same order as that found for the experimental spectra (λ_{max}, **2** > **3** > **1**; Figure S14 in the SI). The band that falls in the vis−NIR region is due to the HOMO−LUMO transition and has MMLLCT character, similar to that observed for other diiminedithiolate[14b,44,46] and mixed-ligand dithiolene complexes.[19−21]

TDDFT calculations have also been done in several simulated solvent electric fields, such as DMF, CH_3CN, acetone, CH_2Cl_2, and $CHCl_3$ (Tables S5−S7 in the SI) in order to investigate the effect of the solvent polarity on the electronic transitions and simulate the solvatochromic behavior of the compounds (Figures S15−S18 in the SI). The negative solvatochromism is qualitatively well reproduced even though slightly underestimated.

Although B3LYP is probably the most widely used functional in DFT calculations on transition-metal complexes, we performed additional calculations with two other functionals, CAM-B3LYP[38] and PBE1PBE,[39] with the aim of investigating whether they make better predictions of the electronic transition energies and oscillator strengths in comparison with B3LYP. The geometries were optimized starting from the *ArgusLab*[41]-generated input files. In the case of complex **1**, the calculated geometries are planar, in agreement with the X-ray data (Figure S19 in the SI) and differing from the results obtained with B3LYP. In Table S8 in the SI, a comparison of HOMO−LUMO transition wavelengths, oscillator strengths, and dipole moments calculated in the gas phase and DMF by TDDFT methods with the three different functionals is reported. Taking into account the measured λ_{max}, PBE1PBE made the best predictions of the transitions energies, with a relatively small underestimation, whereas CAM-B3LYP calculated energies larger than those found experimentally. Moreover, the dipole moments calculated by this functional are bigger than those obtained from the others. All of these findings suggest that with CAM-B3LYP the electronic delocalization in the frontier orbitals is smaller compared to that of the other functionals.

In order to evaluate β_0, the differences between the dipole moments of the excited states and those of the ground states ($\Delta\mu_{ge}$) were calculated[43] in the gas phase and in DMF. The calculated values in the gas phase (DMF) are −5.8 (−4.5), −6.4 (−4.7), and −6.7 (−5.5) D for complexes **1**−**3**, respectively. The oscillator strengths (f) and ground-state dipole moments, in the gas phase and in several solvents with different polarity, have been calculated by TDDFT methods and are reported in Table S7 in the SI. In all of the solvents and in the gas phase, complex **2** shows the smallest value of f ($f_3 > f_1 > f_2$), whereas it exhibits the highest molar extinction coefficient for the lowest electronic transition ($\varepsilon_2 > \varepsilon_3 > \varepsilon_1$). The oscillator strengths have also been calculated in both the gas phase and DMF, using other DFT functionals (CAM-B3LYP and PBE1PBE); however, the same sequence in the f values has been found (see Table S8 in the SI).

The values of the first hyperpolarizability were estimated by applying the equation derived from the two-state model[23] (eq 1). The order of the calculated values of β_0 in DMF is **3** > **2** > **1**, whereas it is **2** > **3** > **1** in the gas phase (Table S10 in the SI). The same differences are observed in the trends of calculated $\mu\beta_0$, as well as between the measured values and those calculated in DMF. These mismatches are probably due to the underestimated value of f_2 and to the oversimplified model applied, which is, however, still very useful to easily predict the effect on the β value due to substituents on the ligands.

CONCLUSIONS AND PERSPECTIVES

We have synthesized three new planar push−pull nickel(II) complexes based on dithiolene and diimine ligands. Electronic structural characterization through electrochemical, spectroscopic, and computational methods has shown the low-energy optical transition to be HOMO−LUMO in character from an orbital based on the dithiolene ligand to an orbital based on the diimine ligand. In particular, we have used carboxylate substitution on the diimine (bpy) ligand to red shift the absorption by lowering the LUMO energy and to enhance the transition intensity. Both of these characteristics are expected to increase the first hyperpolarizability according to the two-state model, and indeed this enhancement was observed through EFISH measurements. Notably, the β values are among the highest for square-planar complexes and comparable with related platinum complexes, despite the fact that complexes of the latter metal in general show higher values than those for nickel. These results give guidance toward further enhancement of the second-order NLO characteristics of such complexes through modification of the substituents on the ligands.

ASSOCIATED CONTENT

Supporting Information

X-ray crystallographic data in CIF format, crystal packing structures, solvatochromic effects, OTTLE, DFT-optimized geometries, DFT calculations, frontier orbitals, energy level diagrams, and TDDFT assignments. This material is available free of charge via the Internet at http://pubs.acs.org.

AUTHOR INFORMATION

Corresponding Authors

*pilialuc@unica.it.
*neil.robertson@ed.ac.uk.

Notes

The authors declare no competing financial interest.

ACKNOWLEDGMENTS

L.P. thanks the FP-7 PEOPLE-Marie Curie Intra European Programme and gratefully acknowledges the Sardinia Regional Government for financial support (P.O.R. Sardegna F.S.E. Operational Programme of the Autonomous Region of Sardinia, European Social Fund 2007−2013, Axis IV Human

Resources, Objective l.3, Line of Activity l.3.1 "Avviso di chiamata per il finanziamento di Assegni di Ricerca"). The authors are grateful to Dr. Christopher Cameron and the University of Edinburgh Crystallography service for collecting crystallographic data and solving the crystal structure.

REFERENCES

(1) (a) Zyss, J. *Nonlinear Optical Properties*; Academic Press: New York, 1994. (b) Chemla, D. S., Zyss, J., Eds. *Nonlinear Optical Properties of Organic Molecules and Crystals*; Academic Press: New York, 1987; Vols. *I* and *II*. (c) Marder, S. R., Stucky, G. D., Eds. *Materials for Nonlinear Optics, Chemical Perspectives*; American Chemical Society: Washington, DC, 1991. (d) Marks, T. J.; Ratner, M. A. *Angew. Chem.* **1995**, 167. (e) Coe, B. J. In *Comprehensive Coordination Chemistry II*; McCleverty, J. A., Meyer, T. J., Eds.; Elsevier Pergamon: Oxford, U.K., 2004; Vol. *9*, p 621. (f) Di Bella, S. *Chem. Soc. Rev.* **2001**, *30*, 355. (g) Lacroix, P. *Eur. J. Inorg. Chem.* **2001**, 339. (h) Coe, B. J. In *Nonlinear Optical Properties of Matter: From Molecules to Condensed Phases*; Papadopoulos, M. G., Leszczynski, J., Sadlej, A. J., Eds.; Springer: Dordrecht, The Netherlands, 2006; p 571. (i) Maury, O.; Le Bozec, H. *Acc. Chem. Res.* **2005**, *38*, 691. (j) Coe, B. J. *Coord. Chem. Rev.* **2013**, *257*, 1438.

(2) (a) Prasad, P. N.; Williams, D. J. *Introduction to Nonlinear Optical Effects in Molecules and Polymers*; John Wiley & Sons, Inc.: New York, 1991. (b) Marks, T. J.; Ratner, M. A. *Angew. Chem.* **1995**, 167. (c) Ahlheim, M.; Barzoukas, M.; Bedworth, P. V.; Blanchard-Desce, M.; Fort, A.; Hu, Z.-Y.; Marder, S. R.; Perry, J. M.; Runser, C.; Staehelin, M.; Zysset, B. *Science* **1996**, *271*, 335. (d) Frattarelli, D.; Schiavo, M.; Facchetti, A.; Ratner, M. A.; Marks, T. J. *J. Am. Chem. Soc.* **2009**, *131*, 12595.

(3) (a) Coe, B. J. In *Comprehensive Coordination Chemistry II*; McCleverty, J. A., Meyer, T. J., Eds.; Elsevier Pergamon: Oxford, U.K., 2004; Vol. *9*, p 621. (b) Di Bella, S. *Chem. Soc. Rev.* **2001**, *30*, 355. (c) Lacroix, P. *Eur. J. Inorg. Chem.* **2001**, 339. (d) Coe, B. J. In *Nonlinear Optical Properties of Matter: From Molecules to Condensed Phases*; Papadopoulos, M. G., Leszczynski, J., Sadlej, A. J., Eds.; Springer: Dordrecht, The Netherlands, 2006; p 571. (e) Coe, B. J. *Coord. Chem. Rev.* **2013**, *257*, 1438. (f) Zyss, J. *J. Chem. Phys.* **1993**, *98*, 6583. (g) Zyss, J.; Ledoux, I. *Chem. Rev.* **1994**, *94*, 77. (h) Maury, O.; Le Bozec, H. *Acc. Chem. Res.* **2005**, *38*, 691.

(4) Coe, B. J.; Houbrechts, S.; Asselberghs, I.; Persoons, A. *Angew. Chem., Int. Ed.* **1999**, *38*, 366.

(5) (a) Clays, K.; Hendrickx, E.; Triest, M.; Verbiest, T.; Persoon, A.; Dehu, C.; Bredas, J. L. *Science* **1993**, *262*, 1419. (b) Costes, J. P.; Lamere, J. F.; Lepetit, C.; Lacroix, P.; Dahan, F.; Nakatani, K. *Inorg. Chem.* **2005**, *44*, 1973. (c) Sanguinet, L.; Pozzo, J.-L.; Guillaume, M.; Champagne, B.; Castet, F.; Ducasse, L.; Maury, E.; Soulié, J.; Mançois, F.; Adamietz, F.; Rodriguez, V. *J. Phys. Chem. B* **2006**, *110*, 10672.

(6) (a) Nakatani, K.; Delaire, J. *Chem. Mater.* **1997**, *9*, 2682. (b) Aubert, V.; Guerchais, V.; Ishow, E.; Hoang-Thi, K.; Ledoux, I.; Nakatani, K. *Angew. Chem., Int. Ed.* **2008**, *47*, 577. (c) Song, P.; Gao, A. H.; Zhou, P. W.; Chu, T. S. *J. Phys. Chem. A* **2012**, *116*, 5392.

(7) (a) Champagne, B.; Spassanova, M.; Jadin, J. B.; Kirtman, B. *J. Chem. Phys.* **2012**, *134*, 8101. (b) Champagne, B.; Plaquet, A.; Pozzo, J.-L.; Rodriguez, V.; Castet, F. *J. Am. Chem. Soc.* **2012**, *134*, 8101.

(8) (a) Coe, B. J. *Acc. Chem. Res.* **2006**, *39*, 383. (b) Broubekeur-Lecaque, L.; Coe, B. J.; Harris, A. J.; Helliwell, M.; Asselberghs, I.; Clays, K.; Foerier, S.; Verbiest, T. *Inorg. Chem.* **2011**, *50*, 12886. (c) Liu, C. G.; Su, Z. M.; Guan, X. H.; Muhammad, S. *J. Phys. Chem. C* **2011**, *115*, 23946.

(9) (a) Verbiest, T.; Sioncke, S.; Persoons, A.; Vyklicky, L.; Katz, T. J. *Angew. Chem., Int. Ed.* **2002**, *41*, 3882. (b) Lamere, J. F.; Lacroix, P. G.; Farfan, N.; Rivera, J. M.; Santillan, R.; Nakatani, K. *J. Mater. Chem.* **2006**, *16*, 2913.

(10) (a) Lacroix, P. G.; Clément, R.; Nakatani, K.; Zyss, J.; Ledoux, I. *Science* **1994**, *263*, 658. (b) Lacroix, P. G.; Malfant, I.; Bénard, S.; Yu, P.; Rivière, E.; Nakatani, K. *Chem. Mater.* **2001**, *13*, 441. (c) Train, C.; Nuida, T.; Gheorghe, R.; Gruselle, M.; Ohkoshi, S. *J. Am. Chem. Soc.* **2009**, *131*, 16838. (d) Pinkowicz, D.; Podgajny, R.; Nitek, W.; Rams, M.; Majcher, A. M.; Nuida, T.; Ohkoshi, S.; Sieklucka, B. *Chem. Mater.* **2011**, *23*, 21. (e) Lacroix, P. G.; Malfant, I.; Real, J.-A.; Rodriguez, V. *Eur. J. Inorg. Chem.* **2013**, 615.

(11) (a) Pap, J. S.; Benedito, F. L.; Bothe, E.; Bill, E.; De Beer George, S.; Weyhermuller, T.; Wieghardt, K. *Inorg. Chem.* **2007**, *46*, 4187. (b) Smucker, B. W.; Hudson, J. M.; Omary, M. A.; Dunbar, K. R. *Inorg. Chem.* **2003**, *42*, 4714.

(12) (a) Cummings, S. D., Eisenberg, R., Stiefel, E. I. Eds. Dithiolene Chemistry: Synthesis, Properties, and Applications. *Progress in Inorganic Chemistry*; Wiley: Chichester, U.K., 2004; Vol. *52*, pp 315−367. (b) Cummings, S. D.; Cheng, L.-T.; Eisenberg, R. *Chem. Mater.* **1997**, *9*, 440.

(13) (a) Zuleta, J. A.; Burberry, M. S.; Eisenberg, R. *Coord. Chem. Rev.* **1990**, *97*, 47. (b) Cummings, S. D.; Eisenberg, R. *J. Am. Chem. Soc.* **1996**, *118*, 1949. (c) Zuleta, J. A.; Burberry, M. S.; Eisenberg, R. *Coord. Chem. Rev.* **1991**, *111*, 237. (d) Weinstein, J. A.; Tierney, M. T.; Davies, E. S.; Base, K.; Robeiro, A. A.; Grinstaff, M. A. *Inorg. Chem.* **2006**, *45*, 4544. (e) Vogler, A.; Kunkely, H. *J. Am. Chem. Soc.* **1981**, *103*, 1559.

(14) (a) Makedonas, C.; Mitsopoulou, C. A.; Lahoz, F. J.; Balana, A. I. *Inorg. Chem.* **2003**, *42*, 8853. (b) Makedonas, C.; Mitsopoulou, C. A. *Inorg. Chim. Acta* **2007**, *360*, 3997.

(15) (a) Geary, E. A. M.; Hirata, N.; Clifford, J.; Durrant, J.; Parson, S.; Dawson, A.; Yellowlees, L. J.; Robertson, N. *Dalton Trans.* **2003**, 3757. (b) Geary, E. A. M.; Yellowlees, L. J.; Jack, L. A.; Parson, S.; Hirata, N.; Durrant, J.; Robertson, N. *Inorg. Chem.* **2005**, *44*, 242.

(16) Zhang, J.; Du, P.; Schneider, J.; Jarosz, P.; Eisenberg, R. *J. Am. Chem. Soc.* **2007**, *129*, 7726.

(17) Chen, C.-T.; Liao, S.-Y.; Lin, K.-J.; Chen, C.-H.; Lin, T-Y. J. *Inorg. Chem.* **1999**, *38*, 2734.

(18) (a) Chen, C.-T.; Liao, S.-Y.; Lin, K.-J.; Lai, L.-L. *Adv. Mater.* **1998**, *3*, 335. (b) Bigoli, F.; Chen, C.-T.; Deplano, P.; Mercuri, M. L.; Pellinghelli, M. A.; Pilia, L.; Pintus, G.; Serpe, A.; Trogu, E. F. *Chem. Commun.* **2001**, 2246. (c) Curreli, S.; Deplano, P.; Faulmann, C.; Ienco, A.; Mealli, C.; Mercuri, M. L.; Pilia, L.; Pintus, G.; Serpe, A.; Trogu, E. F. *Inorg. Chem.* **2004**, *43*, 5069. (d) Deplano, P.; Mercuri, M. L.; Serpe, A.; Pilia, L. In Zabicky, J., Ed. *The Chemistry of Metal Enolates*, John Wiley & Sons, Ltd.: New York, 2009; p 879. (e) Deplano, P.; Marchio, L.; Artizzu, F.; Mercuri, M. L.; Pilia, L.; Pintus, G.; Serpe, A.; Yagubskii, E. B. *Monatsh. Chem.* **2009**, *140*, 775. (f) Pilia, L.; Artizzu, F.; Faulmann, C.; Mercuri, M. L.; Serpe, A.; Deplano, P. *Inorg. Chem. Commun.* **2009**, *12*, 490. (g) Deplano, P.; Pilia, L.; Espa, D.; Mercuri, M. L.; Serpe, A. *Coord. Chem. Rev.* **2010**, *254*, 1434.

(19) (a) Pilia, L.; Espa, D.; Barsella, A.; Fort, A.; Mitsopoulou, C. A.; Marchio, L.; Mercuri, M. L.; Serpe, A.; Makedonas, C.; Deplano, P. *Inorg. Chem.* **2011**, *50*, 10015. (b) Espa, D.; Pilia, L.; Marchio, L.; Mercuri, M. L.; Serpe, A.; Barsella, A.; Fort, A.; Dalgleish, S. J.; Robertson, N.; Deplano, P. *Inorg. Chem.* **2011**, *50*, 2058.

(20) (a) Espa, D.; Pilia, L.; Marchio, L.; Artizzu, F.; Mercuri, M. L.; Serpe, A.; Simão, D.; Almeida, M.; Pizzotti, M.; Tessore, F.; Deplano, P. *Dalton Trans.* **2012**, *41*, 3485. (b) Espa, D.; Pilia, L.; Marchio, L.; Pizzotti, M.; Robertson, N.; Tessore, F.; Mercuri, M. L.; Serpe, A.; Deplano, P. *Dalton Trans.* **2012**, *41*, 12106.

(21) Espa, D.; Pilia, L.; Mercuri, M. L.; Serpe, A.; Marchio, L.; Barsella, A.; Fort, A.; Makedonas, C.; Mitsopoulou, C. A.; Deplano, P. *Inorg. Chem.* **2014**, *53*, 1170.

(22) (a) Chen, C.-T.; Liao, S.-Y.; Lin, K.-J.; Lin, T.-Y. J.; Lia, L.-L.; Chen, C.-H. *Nonlinear Opt.* **1999**, *22*, 35. (b) Chen, C.-T.; Lin, T.-Y. J.; Chen, C.-H.; Lin, K.-J. *J. Chin. Chem. Soc.* **2000**, *47*, 197.

(23) (a) Oudar, J. *J. Chem. Phys.* **1977**, *67*, 446. (b) Oudar, J.; Chemla, D. S. *J. Chem. Phys.* **1997**, *66*, 2664. (c) Bruni, S.; Cariati, E.; Cariati, F.; Porta, F. A.; Quici, S.; Roberto, D. *Spectrochim. Acta, Part A* **2011**, *57*, 1417. (d) Moylan, C. R.; Twieg, R. J.; Lee, V. Y.; Swanson, S. A.; Betterton, K. M.; Miller, R. D. *J. Am. Chem. Soc.* **1993**, *115*, 12599.

(24) Dalgleish, S.; Labram, J. G.; Li, Z.; Wang, J.; McNeill, C. R.; Anthopoulos, T. D.; Greenham, N. C.; Robertson, N. *J. Mater. Chem.* **2011**, *21*, 15422.
(25) Zhang, K. Y.; Lo, K. K.-W. *Inorg. Chem.* **2009**, *48*, 6011.
(26) Hartke, K.; Kissel, T.; Quante, J.; Matusch, R. *Chem. Ber.* **1980**, *113*, 1898.
(27) Brewer, B.; Brooks, N. R.; Abdul-Halim, S.; Sykes, A. G. *J. Chem. Cryst.* **2003**, *33*, 651.
(28) Cariati, E.; Pizzotti, M.; Roberto, D.; Tessore, F.; Ugo, R. *Coord. Chem. Rev.* **2006**, *250*, 1210 and references cited therein.
(29) *SMART (control) and SAINT (integration) software for CCD systems*; Bruker AXS: Madison, WI, 1994.
(30) Sheldrick, G. M. *SADABS*, version 2.04; University of Göttingen: Göttingen, Germany, 2001.
(31) Altomare, A.; Cascarano, G.; Giacovazzo, C.; Guagliardi, A.; Burla, M. C.; Polidori, G.; Camalli, M. *J. Appl. Crystallogr.* **1994**, *27*, 435.
(32) Watkin, D. J.; Prout, C. K.; Carruthers, J. R.; Betteridge, P. W.; Cooper, R. I. *CRYSTALS*; Chemical Crystallography Laboratory: Oxford, U.K., 2003; Issue 12.0.
(33) Macrae, C. F.; Edgington, P. R.; McCabe, P.; Pidcock, E.; Shields, G. P.; Taylor, R.; Towler, M.; van de Streek, J. *J. Appl. Crystallogr.* **2006**, *39*, 453.
(34) Parr, R. G.; Yang, W. *Density Functional Theory of Atoms and Molecules*; Oxford University Press: Oxford, U.K., 1989.
(35) Frisch, M. J.; Trucks, G. W.; Schlegel, H. B.; Scuseria, G. E.; Robb, M. A.; Cheeseman, J. R.; Scalmani, G.; Barone, V.; Mennucci, B.; Petersson, G. A.; Nakatsuji, H.; Caricato, M.; Li, X.; Hratchian, H. P.; Izmaylov, A. F.; Bloino, J.; Zheng, G.; Sonnenberg, J. L.; Hada, M.; Ehara, M.; Toyota, K.; Fukuda, R.; Hasegawa, J.; Ishida, M.; Nakajima, T.; Honda, Y.; Kitao, O.; Nakai, H.; Vreven, T.; Montgomery, J. A., Jr.; Peralta, J. E.; Ogliaro, F.; Bearpark, M.; Heyd, J. J.; Brothers, E.; Kudin, K. N.; Staroverov, V. N.; Kobayashi, R.; Normand, J.; Raghavachari, K.; Rendell, A.; Burant, J. C.; Iyengar, S. S.; Tomasi, J.; Cossi, M.; Rega, N.; Millam, N. J.; Klene, M.; Knox, J. E.; Cross, J. B.; Bakken, V.; Adamo, C.; Jaramillo, J.; Gomperts, R.; Stratmann, R. E.; Yazyev, O.; Austin, A. J.; Cammi, R.; Pomelli, C.; Ochterski, J. W.; Martin, R. L.; Morokuma, K.; Zakrzewski, V. G.; Voth, G. A.; Salvador, P.; Dannenberg, J. J.; Dapprich, S.; Daniels, A. D.; Farkas, Ö.; Foresman, J. B.; Ortiz, J. V.; Cioslowski, J.; Fox, D. J. *Gaussian 09*, revision D.01; Gaussian, Inc.: Wallingford, CT, 2009.
(36) Becke, A. D. *J. Chem. Phys.* **1993**, *98*, 5648.
(37) Lee, C.; Yang, W.; Parr, R. G. *Phys. Rev. B* **1988**, *37*, 785.
(38) (a) Hay, P. J.; Wadt, W. R. *J. Chem. Phys.* **1985**, *82*, 270. (b) Hay, P. J.; Wadt, W. R. *J. Chem. Phys.* **1985**, *82*, 299.
(39) (a) Barone, V.; Cossi, M. *J. Phys. Chem. A* **1998**, *102*, 1995. (b) Cossi, M.; Rega, N.; Scalmani, G.; Barone, V. *J. Comput. Chem.* **2003**, *24*, 669.
(40) (a) Krishnan, R.; Binkley, J. S.; Seeger, R.; Pople, J. A. *J. Chem. Phys.* **1980**, *72*, 650. (b) McLean, A. D.; Chandler, G. S. *J. Chem. Phys.* **1980**, *72*, 5639.
(41) Thompson, M. A. *ArgusLab 4.0.1*; Planaria Software LLC: Seattle, WA, 2012; http://www.arguslab.com/arguslab.com/ArgusLab.html/.
(42) Barone, V.; Cossi, M.; Tomasi, J. *J. Phys. Chem. A* **1997**, *107*, 3210.
(43) Cappel, U. B.; Feldt, S. M.; Schöneboom, J.; Hagfeldt, A.; Boschloo, G. *J. Am. Chem. Soc.* **2010**, *132*, 9096.
(44) Cocker, T. M.; Bachman, R. E. *Inorg. Chem.* **2001**, *40*, 1550.
(45) The cyclic voltammetry measurements reported in ref 33 were performed in benzonitrile solutions, and the data are reported relative to the Fc/Fc^+ couple; for the sake of comparison, these electrochemical potentials were shifted to those with $Ag/AgCl_{sat.}$ as the reference electrode using the reduction potential value reported in the paper: Noviandri, I.; Brown, K. N.; Fleming, D. S.; Gulyas, P. T.; Lay, P. A.; Masters, A. F.; Phillips, L. *J. Phys. Chem. B* **1999**, *103* (32), 6713.
(46) Base, K.; Tierney, M. T.; Fort, A.; Muller, J.; Grinstaff, M. W. *Inorg. Chem.* **1999**, *38*, 287.